From Q-space to R-space: Introduction to atomic and magnetic PDF-analysis

Henry E. Fischer

Institut Laue-Langevin, Grenoble

Structure Group talk, MLZ (FRM-II),
Wednesday 11 May 2022

Diffraction Basics

Schematic of a diffraction measurement (mono-λ)

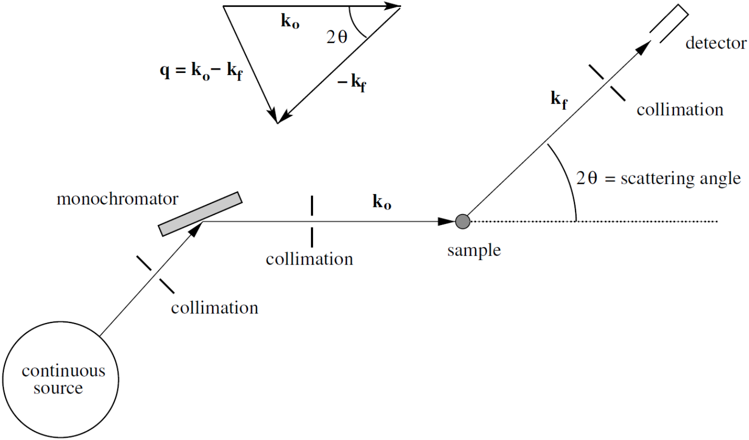

Quanta (*e.g.* x-rays or neutrons) of incident wavevector $\mathbf{k}_\mathrm{o}$ and incident energy E_o are scattered by a sample through a scattering angle 2θ thus losing kinetic energy $\hbar\omega = E_\mathrm{o} - E_\mathrm{f}$ and momentum $\hbar\mathbf{q}$ where $\mathbf{q} = \mathbf{k}_\mathrm{o} - \mathbf{k}_\mathrm{f}$ is the wavevector transfer or scattering vector.

Schematic of a diffraction measurement (mono-λ)

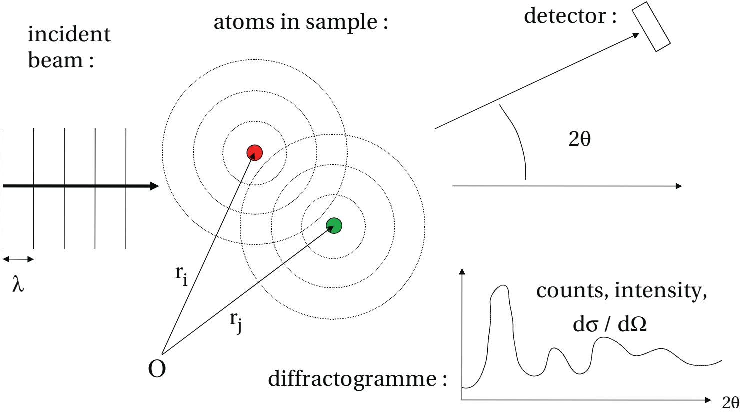

The spherical waves of scattering amplitude from all the atoms in a given quantum's coherence volume ($\phi \sim 100$ Å) interfere with each other at the detector, producing a diffraction pattern as a function of the scattering angle 2θ or the scalar $q = (4\pi/\lambda)\sin(\theta)$.

Coherence volume for a scattered quantum

For each particle/wave emitted by an incoherent source of transverse FWHM size H by V, scattered by a sample at a distance L and then detected, purely geometric considerations impose a limit to the size of the scattering region within the sample over which a given quantum's scattered (from different atoms) amplitudes can be added coherently.

Assuming for convenience a Gaussian wavepacket for the incident quantum (*e.g.* x-ray or neutron), the Uncertainty Principle can be used to relate the standard deviations of its position and wavenumber:

$$\delta x_j \, \delta k_j = 1/2 \quad \text{since} \quad \delta x_j \, \delta p_j = \hbar/2$$

where the dimensions $j = h, v$ are transverse to the incident beam while $j = l$ is parallel (*i.e.* longitudinal). In terms of FWHM for the wavepacket:

$$\xi_j \, \Delta k_j = \frac{4 \ln(4)}{2} \quad \Rightarrow \quad \xi_j = \frac{5.55}{2 \, \Delta k_j}$$

where the mutually orthogonal *coherence lengths* ξ_j are the FWHM dimensions of the (roughly ellipsoidal) *coherence volume* $V_{\text{coh}} = \xi_h \xi_v \xi_l$ from which the quantum scattered somewhere in the sample.

Coherence volume for a scattered quantum (cont'd)

The Δk_j are given by the collimation FWHM's (small angle approx.) and by the monochromaticity (FWHM $\Delta\lambda$) of the incident beam:

$$\Delta k_{h,v} = \frac{2\pi}{\lambda}\frac{H,V}{L} \quad \text{and} \quad \Delta k_l = \frac{2\pi}{\lambda}\frac{\Delta\lambda}{\lambda}$$

and thus the 3 coherence lengths:

$$\xi_{h,v} = \lambda\frac{\ln(4)}{\pi}\frac{L}{H,V} = 0.44\,\lambda\frac{L}{H,V} \quad \text{and} \quad \xi_l = 0.44\,\lambda\frac{\lambda}{\Delta\lambda}$$

increase as the collimation+monochromaticity ⇒ resolution improve.

NB: In general, the sample-to-detector optics (*e.g.* α_3 collimation) also contribute to the instrumental resolution function of the diffraction pattern. In spite of occuring after the scattering event, such a *post-selection* of the scattered quanta leads to additional and complementary expressions in the above formulæ for ξ_j.

In the simplistic case of a constant-ish FWHM resolution of Δq for the final diffraction pattern, the FWHM coherence length in the diffraction plane of the scattering vector $\mathbf{q}$ is simply $\xi_q = 5.55/\Delta q$.

Coherence volume of a neutron wavepacket

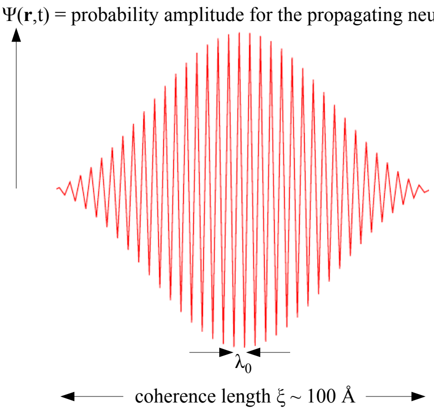

$\Psi(\mathbf{r},t)$ = probability amplitude for the propagating neutron's presence

λ_0

coherence length $\xi \sim 100$ Å

$|\Psi(\mathbf{r},t)|^2$ = probability of finding the neutron at position **r** at time t

Propagation direction:

→ $\mathbf{k_0}$ = wavevector

$k_0 = |\mathbf{k_0}| = 2\pi/\lambda_0$

$E_0 = \hbar\omega_0 = \hbar^2 k_0^2 / 2m$

spread in wavelength:

$\Delta\lambda/\lambda = \Delta k/k \sim 1\ \%$

A Gaussian wavepacket of energy $\hbar\omega_0$ is localized in position and wavevector for each dimension as *e.g.* $\Delta x\, \Delta k_x \sim \hbar/2$ and propagates with group velocity $v_g = \mathrm{d}\omega/\mathrm{d}k$. The diffracting neutron has "seen" only the 100,000 or so atoms that "felt" its wavefunction $\Psi(\mathbf{r},t)$ within the coherence volume $V_{\mathrm{coh}} \sim \xi^3$ of the diffraction event.

Interference from 2 diffracting atoms

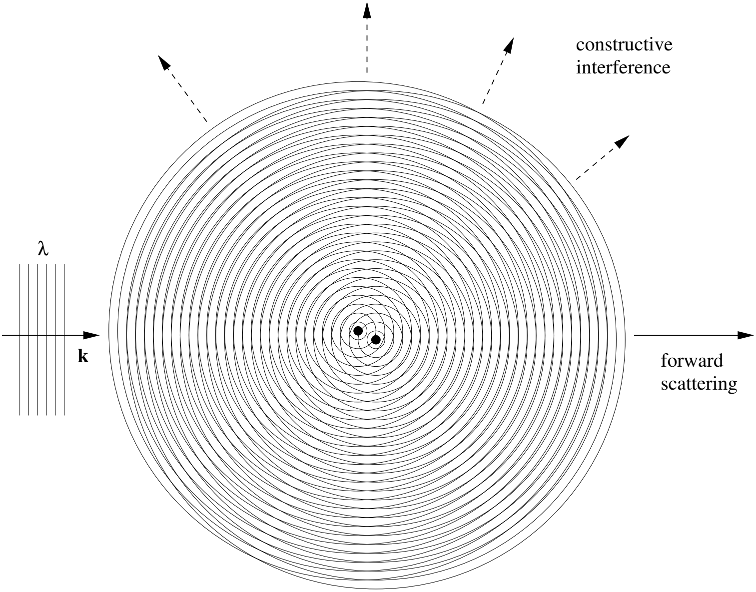

Interference from an ordered line of 3 atoms

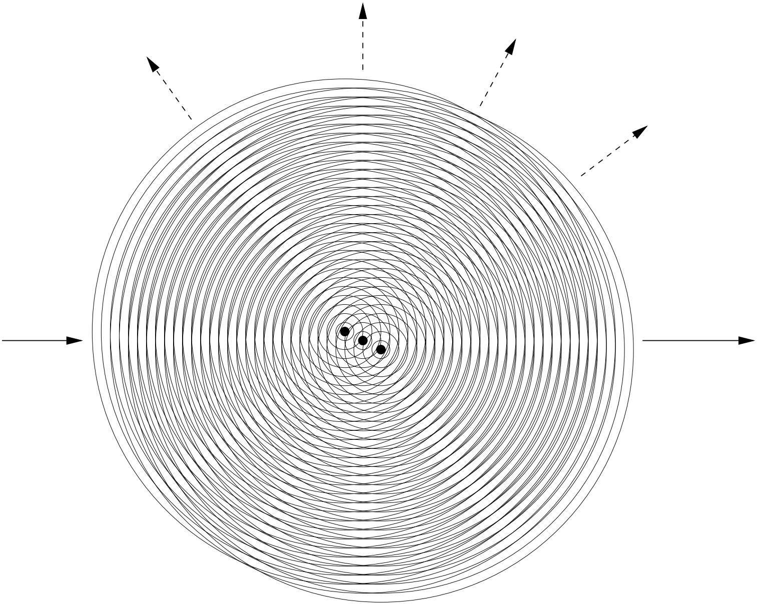

Interference from an ordered array of 9 atoms

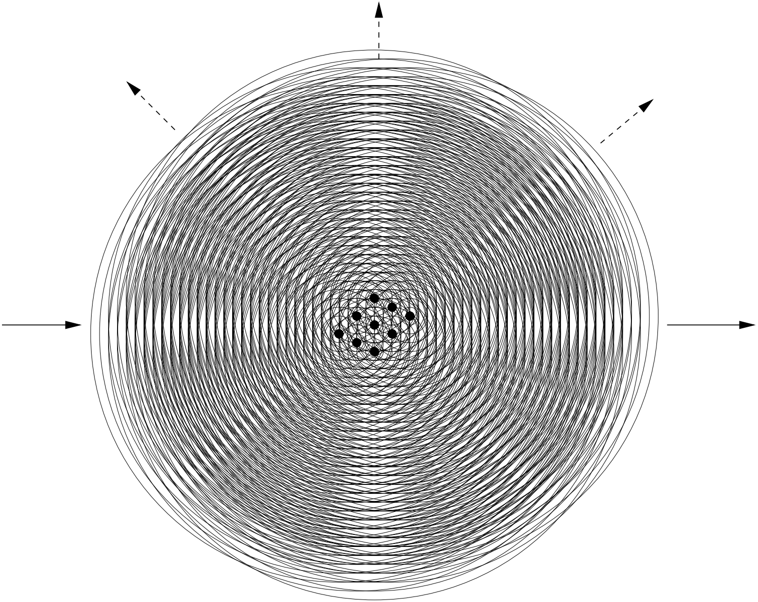

Interference from an ordered array of 9 atoms

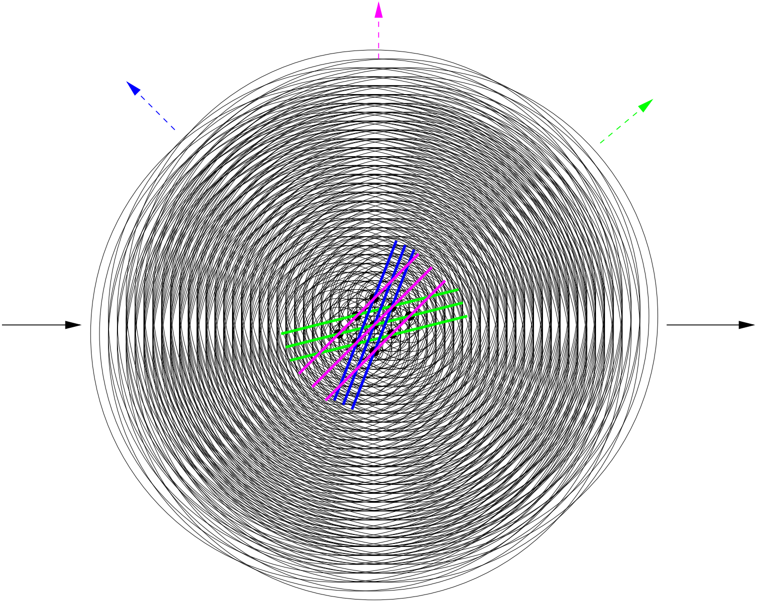

Bragg's Law for diffraction from atomic planes

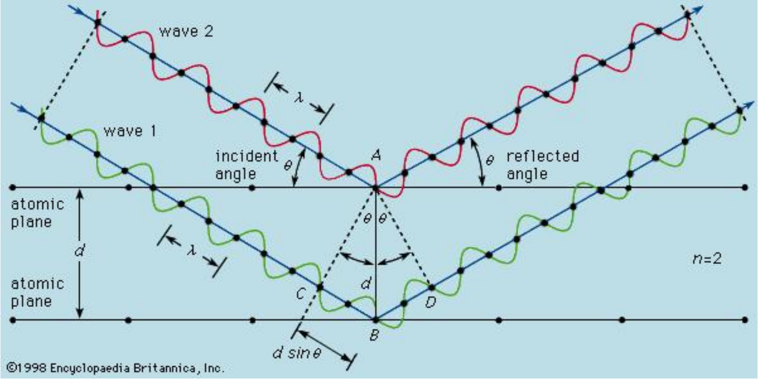

©1998 Encyclopaedia Britannica, Inc.

For elastic scattering ($|\mathbf{k}_\mathrm{f}| = |\mathbf{k}_0| = k = 2\pi/\lambda$), the difference in pathlength between two parts of the (quasi-linear) wavefront, as diffracted or "reflected" by neighboring atomic planes, must be an integral multiple of λ:

$$n\lambda = 2d\,\sin(\theta)$$

and the exit angle must be equal to the incident angle θ, meaning that the wavevector transfer $\mathbf{q}$ is $\perp$ the planes.

Interference from a disordered array of 9 atoms

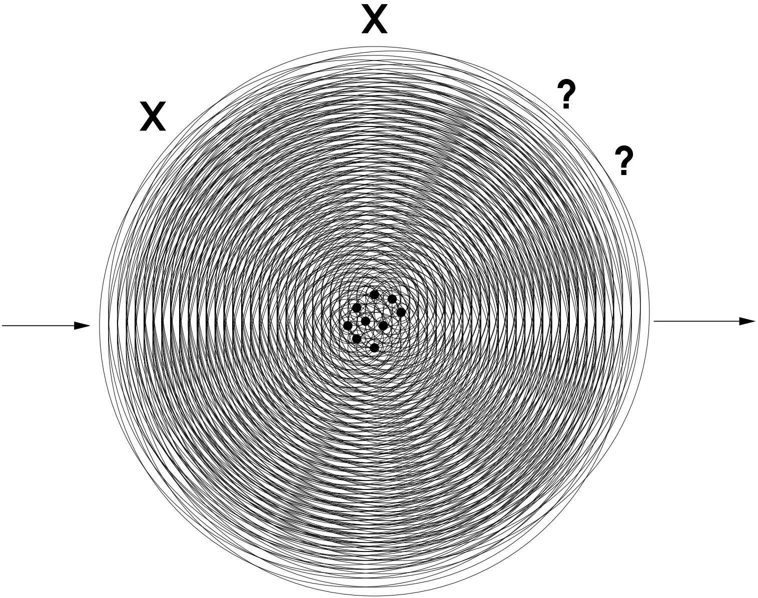

Diffracted intensity from an ensemble of atoms

Constructive interference at the detector results when the path lengths followed by a neutron wave, as scattered by two different atoms, differ by a multiple of λ. This also holds for “reflection” from parallel atomic planes of period *d* as shown by Bragg’s law: $n\lambda = 2d\,\sin(\theta)$.

A pathlength difference of $n\cdot\lambda$ means a phase difference of $n\cdot 2\pi$. So, we can sum up all the scattered amplitudes b_i and phases from all the diffracting atoms (*i.e.* within V_{coh}) at positions $\mathbf{r}_i$ and write the total scattered amplitude propagating along $\mathbf{k}_{\mathrm{f}}$ towards the detector:

$$A_{\mathrm{diff}}(\mathbf{q}) = \sum_i^N b_i\, e^{i\mathbf{q}\cdot\mathbf{r}_i} \qquad b_i = \text{"scattering length"}$$

where $\mathbf{q} = \mathbf{k}_{\mathrm{o}} - \mathbf{k}_{\mathrm{f}}$ as before, and $|\mathbf{k}_{\mathrm{f}}| = |\mathbf{k}_0| = k \Rightarrow$ elastic. The diffracted intensity or counting rate recorded by the detector is then:

$$I(\mathbf{q}) \propto |A_{\mathrm{diff}}(\mathbf{q})|^2 = \left|\sum_i^N b_i\, e^{i\mathbf{q}\cdot\mathbf{r}_i}\right|^2 = \sum_{i,j}^N b_i b_j^*\, e^{i\mathbf{q}\cdot\mathbf{r}_{ij}} \;,$$

where $\mathbf{r}_{ij} = \mathbf{r}_i - \mathbf{r}_j$ is the relative position of atom *i* with respect to atom *j*, and * denotes the complex conjugate.

Diffracted intensity from a periodic structure

The atoms of a crystal are arranged periodically within an ordered array or lattice of unit cells each having dimensions defined by the vectors **a**, **b** and **c**. The identical arrangement of atoms within each unit cell is called the basis or motif. The integer coefficients $u, v, w \in \mathbb{Z}$ thus specify the position of a unit cell within the lattice $\mathbf{r}_{uvw} = u\mathbf{a} + v\mathbf{b} + w\mathbf{c}$, and the fractional coefficients $0 \leq x_m, y_m, z_m < 1$ specify the m^{th} atom's position $\mathbf{r}_m = x_m\mathbf{a} + y_m\mathbf{b} + z_m\mathbf{c}$ within the motif:

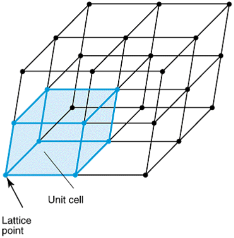

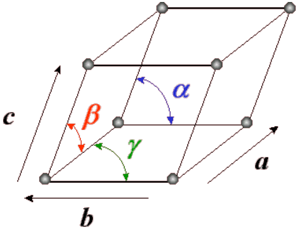

An atom's position in the crystal can then be written as:

$$\mathbf{r}_i = \mathbf{r}_{uvw} + \mathbf{r}_m = (u + x_m)\mathbf{a} + (v + y_m)\mathbf{b} + (w + z_m)\mathbf{c}\ .$$

Diffracted intensity from a periodic structure

We can thus rewrite the sum of scattered amplitudes and phases as:

$$A_{\text{diff}}(\mathbf{q}) = \sum_{i}^{N} b_i\, e^{i\mathbf{q}\cdot\mathbf{r}_i} = \sum_{u,v,w}^{\textbf{lattice}} \sum_{m}^{\textbf{motif}} b_{\text{coh},m}\, e^{i\mathbf{q}\cdot(\mathbf{r}_{uvw}+\mathbf{r}_m)}$$

$$= \left[\sum_{u,v,w}^{\textbf{lattice}} e^{i\mathbf{q}\cdot\mathbf{r}_{uvw}}\right]\cdot\left[\sum_{m}^{\textbf{motif}} b_{\text{coh},m}\, e^{i\mathbf{q}\cdot\mathbf{r}_m}\right] = L(\mathbf{q})\, M(\mathbf{q}) \,,$$

where $b_{\text{coh},m} = \overline{b_i}$ is the scattering length at site m in the motif as averaged over the entire crystal. The complex function $L(\mathbf{q})$ is the form factor of the lattice that gives rise to Bragg peaks as a function of the lattice symmetry, and $M(\mathbf{q})$ is the structure factor of the motif (or basis) that modulates the intensity of the Bragg peaks:

$$I(\mathbf{q}) \propto |A_{\text{diff}}(\mathbf{q})|^2 = |L(\mathbf{q})|^2\, |M(\mathbf{q})|^2$$

$$= \left[\sum_{u,v,w,u',v',w'}^{\textbf{lattice}} e^{i\mathbf{q}\cdot(\mathbf{r}_{uvw}-\mathbf{r}_{u'v'w'})}\right]\cdot\left[\sum_{m,m'}^{\textbf{motif}} b_{\text{coh},m} b^{*}_{\text{coh},m'}\, e^{i\mathbf{q}\cdot(\mathbf{r}_m-\mathbf{r}_{m'})}\right] .$$

Diffracted intensity from a periodic structure

Note that when we consider all lattice positions $\mathbf{r}_{uvw}$ and $\mathbf{r}_{u'v'w'}$ lying within a single plane, then the dot product $\mathbf{q}\cdot(\mathbf{r}_{uvw}-\mathbf{r}_{u'v'w'})=0$ implies that $\mathbf{q}$ is $\perp$ to that plane, consistent with the Bragg condition! *Hmmm.* In fact, it turns out that $\mathbf{q}$ satisfies the Bragg condition if and only if

$$\mathbf{q}\cdot\mathbf{r}_{uvw}=n2\pi \qquad n\in\mathbb{Z},\quad \forall\, u,v,w\in\mathbb{Z}\ .$$

The set of all such $\mathbf{q}$ form a lattice of reciprocal-space vectors:

$$\mathbf{Q}_{hkl}=h\mathbf{a}^{\star}+k\mathbf{b}^{\star}+l\mathbf{c}^{\star} \qquad h,k,l\in\mathbb{Z}\ ,$$

where the reciprocal lattice basis vectors are given by:

$$\mathbf{a}^{\star}=\frac{2\pi}{V_{\mathrm{cell}}}\mathbf{b}\times\mathbf{c}\ ,\qquad \mathbf{b}^{\star}=\frac{2\pi}{V_{\mathrm{cell}}}\mathbf{c}\times\mathbf{a}\ ,\qquad \mathbf{c}^{\star}=\frac{2\pi}{V_{\mathrm{cell}}}\mathbf{a}\times\mathbf{b}\ ,$$

and where V_{cell} is the volume of the real-space unit cell. Note that $\mathbf{a}\cdot\mathbf{a}^{\star}=2\pi$ but $\mathbf{b}\cdot\mathbf{a}^{\star}=\mathbf{c}\cdot\mathbf{a}^{\star}=0$ and likewise for $\mathbf{b}^{\star}$ and $\mathbf{c}^{\star}$. Thus:

$$|L(\mathbf{Q}_{hkl})|^2=\left|\sum_{u,v,w}^{\text{lattice}}e^{i\mathbf{Q}_{hkl}\cdot\mathbf{r}_{uvw}}\right|^2=\left|\sum_{u,v,w}^{\text{lattice}}e^{i2\pi(hu+kv+lw)}\right|^2=P^2$$

where P is the total number of lattice points, whence a Bragg peak.

Laue function for diffraction from *M* atomic planes

The diffraction peaks get sharper and sharper in angle as the number *M* of parallel diffracting crystal planes increases:

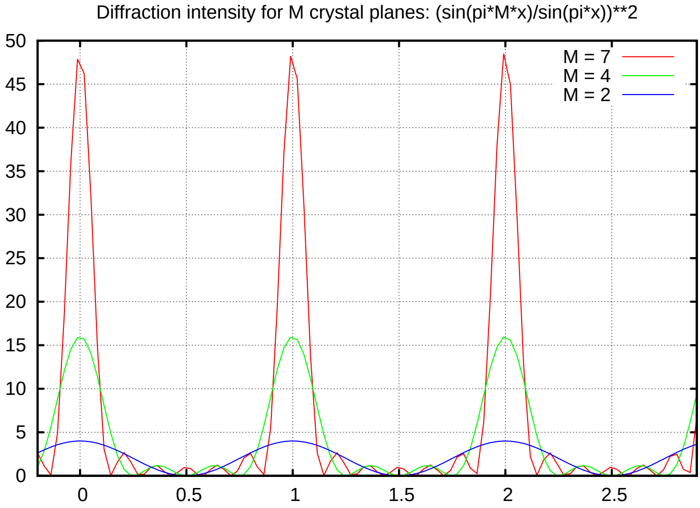

Debye-Waller factor and Thermal Diffuse Scattering

Increased amplitudes of atomic vibration **u** at higher T lead to broader time-averaged "thermal clouds" of atomic positions that reduce Bragg peak intensities via the Debye-Waller factor: $\exp[-\langle(\mathbf{Q}_{hkl}\cdot\mathbf{u})^2\rangle/2]$:

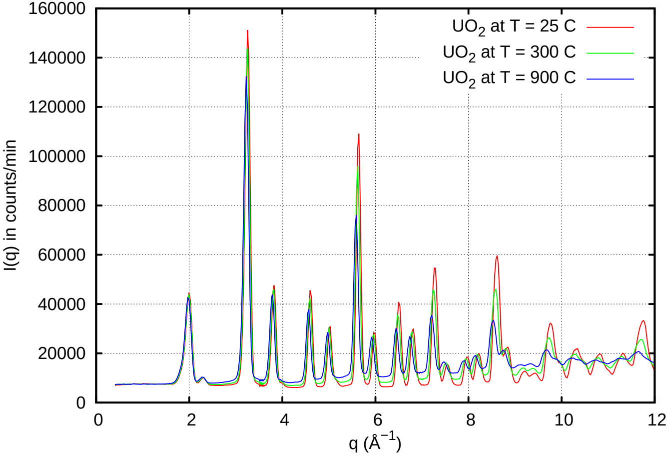

The lost intensity becomes Thermal Diffuse Scattering (TDS) at the base of the Bragg peaks.

Debye-Waller factor and Thermal Diffuse Scattering

The D-W factor (*i.e.* a modulation) reduces the amplitude of a Bragg peak without affecting its width, thus reducing its integrated intensity.

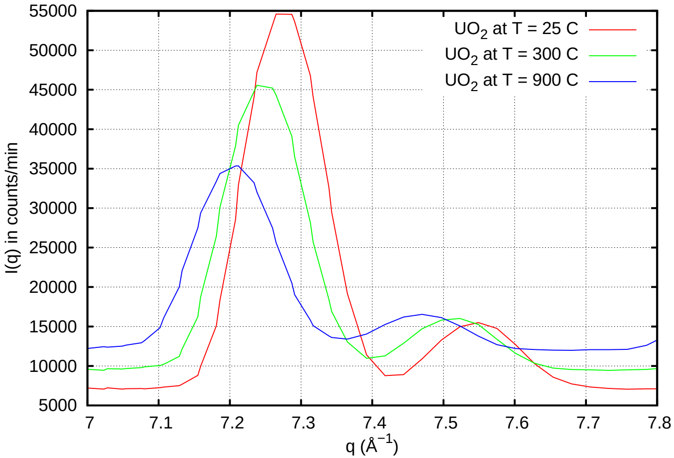

The Bragg peak positions naturally shift to lower *q* as the lattice expands at higher temperature.

The Patterson function as prelude to PDF(r)

If the phases $\phi(hkl)$ of the structure factors $F(hkl)$ were known, one could calculate the scattering length density function $\rho(xyz)$:

$$\rho(xyz) = \frac{1}{V} \sum_{hkl\,-\infty}^{+\infty} |F(hkl)| \,.\, e^{\,-2\pi i[hx+ky+lz-\phi(hkl)]}$$

and thereby deduce the atomic positions x, y, z within the unit cell. By using instead the measured intensity $I(hkl) \propto |F(hkl)|^2$ in the Fourier series, we eliminate $\phi(hkl)$ and obtain the Patterson function $P(uvw)$ of all *interatomic distances* ($u = x_i - x_j$, $v = y_i - y_j$, $w = z_i - z_j$) rather than of all absolute atomic positions in the unit cell:

$$P(uvw) = \frac{1}{V} \sum_{hkl\,-\infty}^{+\infty} |F(hkl)|^2 \,.\cos 2\pi\,[hu + kv + lw]$$

A radial average of $P(uvw)$ produces a 1-D pair-distribution function $P(r)$ based solely on elastic Bragg peak intensities, thus representing the sample's structure as averaged over space and time.

The Patterson function as prelude to PDF(r)

Although $P(uvw)$ has the same unit cell as the crystal's, it contains a high density of peaks and is by definition centrosymmetric. In 2-D:

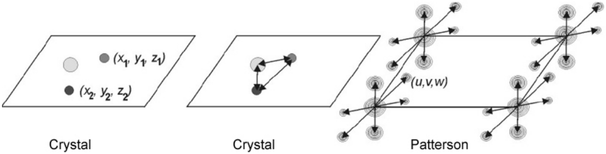

$P(uvw)$ is proportional to the product of the scattering lengths of the pair (or pairs!) of atoms separated by u, v, w, helping to determine their chemical identities. An "average atom" sits at $(uvw) = (000)$:

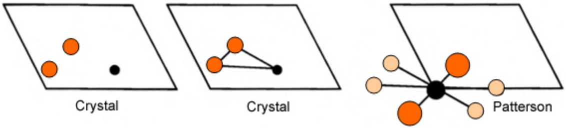

The higher symmetry of $P(uvw)$ is obtained from the crystal symmetry by setting the translational part of all symmetry operators to zero and assuring that each has a center of symmetry. Consequently, there are only 24 Patterson space groups.

Atomic PDF-analysis

Total scattering, $S(\mathbf{q},\omega)$, and time scales

A diffraction pattern integrates over all sample-neutron *E*-transfers:

$$\frac{d\sigma}{d\Omega}(\mathbf{q})\Big|_{\mathrm{meas}} = \int_{-\infty}^{E_o} d(\hbar\omega)\,\frac{\sigma}{4\pi}\,\frac{k_f}{k_o}\,N\,S(\mathbf{q},\omega)\ ,$$

and therefore represents a quasi-instantaneous “snapshot” of the sample’s structure, given the very small coherence time $\tau_{\mathrm{coh}} \sim \hbar/(4E_o)$ (from $\Delta t\,\Delta E = \hbar/2$), as ensemble-averaged over coherence volumes.

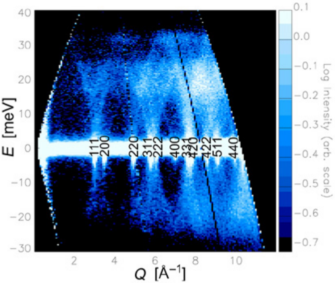

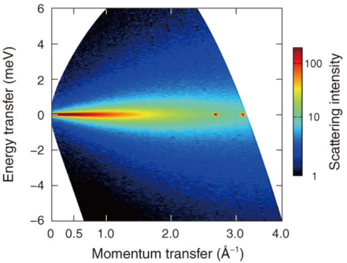

Rietveld refinement of *elastic* Bragg peaks disregards the inelastic scattering containing information about *dynamic* atomic correlations (*e.g.* phonons) and represents the sample’s time-averaged structure.

Total scattering, diffuse intensity, and length scales

In addition, the refinement of diffraction intensity only at Bragg-peak positions neglects the inter-peak diffuse intensity, which when elastic represents time-averaged or *static* local atomic correlations.

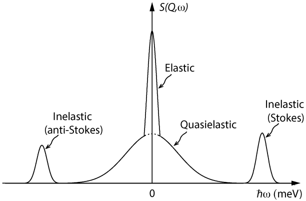

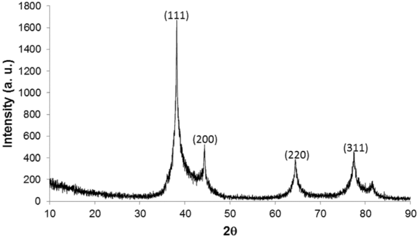

By neglecting the diffuse intensity between (and "under") Bragg peaks, Rietveld refinement additionally performs a spatial average over each neutron coherence volume, resulting in a time+space averaged picture of the sample's structure, which is very useful for crystallography.

By retaining all the original information in the differential cross-section $(d\sigma/d\Omega)(\mathbf{q})$ measured via diffraction, total-scattering represents an ensemble average of quasi-instantaneous snapshots of local structures (*i.e.* within each neutron coherence volume) throughout the sample.

The static approximation for total scattering

When the incident energy E_o exceeds the maximum possible energy transfer $\hbar\omega_\text{max}$ between the scattered quantum and the excitations in the sample, and for $\varepsilon(E_\text{f}) = 1$, it is perfectly valid to use the *static approximation* to derive the *differential scattering cross-section* for diffraction as a function of $\mathbf{q}$ only (note that $k_\text{f} \to k_\text{o} \Rightarrow$ elastic):

$$\frac{d\sigma}{d\Omega}(\mathbf{q}) = \int_{-\infty}^{\omega\to\infty} d\omega \, N \frac{\sigma_s}{4\pi} \, S(\mathbf{q},\omega) \overset{\text{s.a.}}{=} \overline{\left\langle \left| \sum_i^N b_i \, e^{i\mathbf{q}\cdot\mathbf{r}_i} \right|^2 \right\rangle} = \left\langle \sum_{i,j}^N \overline{b_i b_j^*} \, e^{i\mathbf{q}\cdot\mathbf{r}_{ij}} \right\rangle ,$$

where b_i is the scattering length of the i^th atom at position $\mathbf{r}_i$, and $\mathbf{r}_{ij} = \mathbf{r}_i - \mathbf{r}_j$. The $<>$ represent a thermal average and the horizontal bars an ensemble average over the different possible coherence volumes within the sample, each having a particular assignment of scattering lengths in the case of neutron diffraction. Note that scattering lengths are q-dependent in the case of x-ray diffraction (XRD).

When $E_\text{o} < \hbar\omega_\text{max}$, as is often the case for neutron diffraction (ND), the non-satisfaction of the static approximation requires inelasticity corrections to be made to the measured diffraction patterns.

Case of a monoatomic sample (only one Z)

$\Rightarrow (d\sigma/d\Omega)(\mathbf{q})$ measures an *ensemble average* of quasi-instantaneous snapshots of local structures (*i.e.* within the neutron coherence volume) throughout the sample volume over the duration of the experiment.

In neutron scattering, a monoatomic sample can have a distribution of scattering lengths b_i, but there is no correlation between b_i and the structural environment of $\mathbf{r}_i$. The ensemble average over coherence volumes then leads to an expression (units of barns/str/atom) involving a $\mathbf{q}$-dependent coherent term and an isotropic incoherent term:

$$\frac{1}{N}\left[\frac{d\sigma}{d\Omega}(\mathbf{q})\right] = \bar{b}^2 S(\mathbf{q}) + (\overline{b^2} - \bar{b}^2)$$

where the sample's average scattering length $\bar{b} = b_{\mathrm{coh}}$, the scattering cross-section $\sigma_s = 4\pi\overline{b^2}$, and $(\overline{b^2} - \bar{b}^2) = var(b)$ is simply the variance of scattering lengths throughout the sample. The alternative expression:

$$\frac{1}{N}\left[\frac{d\sigma}{d\Omega}(\mathbf{q})\right] = \bar{b}^2\,[S(\mathbf{q}) - 1] + \overline{b^2}$$

comprises a "distinct" term (interference between different atoms) and a "self" term (self-interference from individual atoms).

Case of a monoatomic sample (cont'd)

The *static structure factor* (dimensionless) is then given by

$$S(\mathbf{q}) = \int_{-\infty}^{+\infty} d\omega \;\, S(\mathbf{q},\omega) \;\; = \; \frac{1}{N} \left\langle \sum_{i,j}^{N} e^{i\mathbf{q}\cdot\mathbf{r}_{ij}} \right\rangle$$

and reduces to

$$S(q) = \frac{1}{N} \left\langle \sum_{i,j}^{N} \frac{\sin(qr_{ij})}{(qr_{ij})} \right\rangle$$

in the case of conical Debye-Scherrer diffraction from an isotropic sample (*e.g.* powder, polycrystal, liquid, glass) for which

$$q = |\mathbf{q}| = (4\pi/\lambda)\, \sin(\theta)$$

and 2θ is the diffraction angle with respect to to the incident beam. Finally, for an incident flux Φ and a detector cell of solid angle $d\Omega$, the measured intensity (counts/s) from an isotropic sample is given by

$$I(q) = \Phi\, \frac{d\sigma}{d\Omega}(q)\; d\Omega$$

which, notably, is a function of *q only*.

$S(q)$ for a glass or liquid (isotropic, monoatomic)

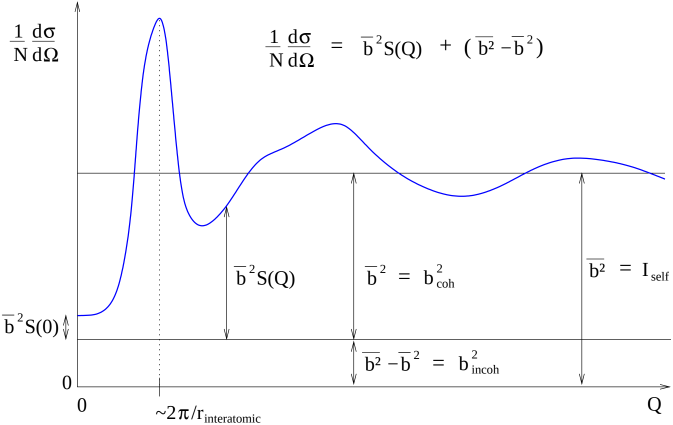

Lack of long-range order, *i.e.* a short structural correlation length, leads to broad peaks in the diffraction pattern of a glass/liquid, and in the case of an ergodic system such as a liquid or gas, there also exists a useful thermodynamic limit: $S(q \to 0) = \rho_0 \chi_T k_B T$ where ρ_0 is the total atomic number density and χ_T is the isothermal compressibility.

Real-space functions (monoatomic case)

Fourier transform gives the *pair-distribution function $g(r)$* which is proportional to the probability of finding an atom at a distance r from an average atom taken as the origin:

$$g(r)-1=\frac{1}{2\pi^2 r\rho_o}\int_0^\infty q\,[S(q)-1]\sin(qr)\,dq$$

in addition to the density function $D(r)$ (also called $G(r)$) used for "PDF-analysis":

$$\mathrm{PDF}(r)=G(r)=D(r)=4\pi r\rho_o\,[g(r)-1]$$

$$=\frac{2}{\pi}\int_0^\infty q\,[S(q)-1]\sin(qr)\,dq$$

as well as the radial distribution function:

$$\mathrm{RDF}(r)=4\pi r^2\rho_o\,g(r)$$

whose integration across peaks yields atomic coordination numbers.

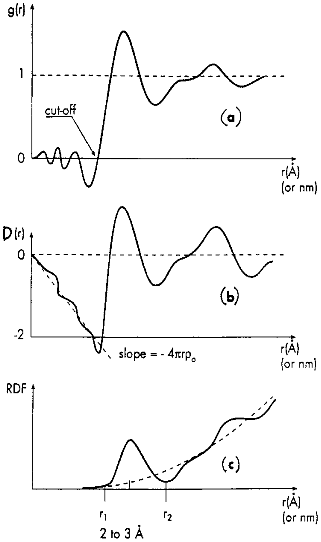

Case of a polyatomic sample (several Z)

In a polyatomic system, the chemical affinities of n different atomic species Z_α necessarily leads to a correlation at atomic sites $\mathbf{r}_i$ between the structural environment and the average scattering length $\overline{b}_\alpha$. This correlation prevents a proper definition of a dimensionless $S(q)$, but the scattered intensity can still be expressed as the sum of a distinct term (the interference function $F(q)$) and a total self-scattering term:

$$\frac{1}{N}\left[\frac{d\sigma}{d\Omega}(q)\right] = \sum_{\alpha,\beta}^{n} c_\alpha c_\beta \overline{b}_\alpha \overline{b}^*_\beta \left[S_{\alpha\beta}(q)-1\right] + \sum_{\alpha}^{n} c_\alpha \overline{b^2}_\alpha \ ,$$

where c_α is the fraction or concentration of atomic species Z_α, and the *partial* structure factor (PSF) $S_{\alpha\beta}(q)$ is the Fourier transform of the *partial* pair-distribution function (PPDF) $g_{\alpha\beta}(r)$, which is in turn proportional to the probability of finding an atom of type Z_β at a distance r from an atom of type Z_α taken as the origin:

$$g_{\alpha\beta}(r) - 1 = \frac{1}{2\pi^2 r \rho_o} \int_0^\infty q\left[S_{\alpha\beta}(q)-1\right]\sin(qr)\, dq \ .$$

Atomic distributions in glass/liquid versus crystal

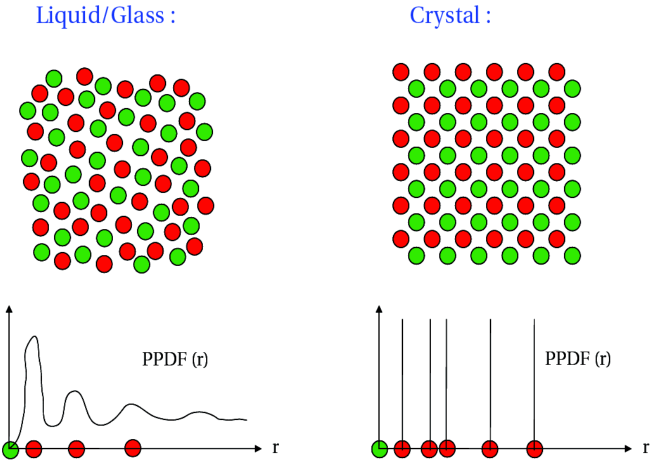
Liquid/Glass :

Crystal :

These *partial* PDFs or PPDFs (*e.g.* from NDIS) represent an ensemble of quasi-instantaneous spatial correlations between red and green atoms: more specifically $g_{GR}(r)$ which is proportional to the average probability of finding a Red atom at a distance r from a Green atom.

The Convolution Theorem

The *convolution* of two functions $f(q)$ and $g(q)$ is given by:

$$f(q) \otimes g(q) = (f \otimes g)(q) = \int_{-\infty}^{\infty} f(q')\, g(q-q')\, dq'$$

where q' is the (dummy) variable of integration.

The *convolution theorem* states that the Fourier Transform (FT) of a convolution is the simply the product of the Fourier Transforms:

$$\mathrm{FT}[f(q) \otimes g(q)] = \mathrm{FT}(f(q))\,\mathrm{FT}(g(q)) = F(r)\, G(r)$$

so that a convolution in q-space gives a modulation in r-space, and vice-versa of course. Therefore deconvolution in q-space should be as simple as FT-ing to r-space, dividing two functions, and then FT-ing back to q-space. For example, if the measured diffraction pattern is $I(q) = f(q) \otimes g(q)$, where $g(q)$ is the real diffraction pattern and $f(q)$ is the known resolution function, then:

$$g(q) = \mathrm{FT}[\,\mathrm{FT}(I(q))\,/\,\mathrm{FT}(f(q))\,]\ .$$

Some useful rules of thumb for Fourier Transforms

The FT of a Gaussian with standard deviation σ_q is also a Gaussian but with standard deviation $\sigma_r = 1/\sigma_q$. And since:

$$\mathrm{HWHM}_q = \mathrm{FWHM_q}/2 = \sqrt{\ln(4)}\,\sigma_q = 1.18\,\sigma_q$$

then the FT of a Gaussian of width FWHM_q is a Gaussian of width

$$\mathrm{FWHM}_r = 4\ln(4)/\mathrm{FWHM}_q = 5.55/\mathrm{FWHM}_q$$

and therefore *not* $2\pi/\mathrm{FWHM}_q$. A sharp resolution function of small FWHM_q for the diffraction data will therefore lead to a broad or gentle modulation of large FWHM_r for the $\mathrm{PDF}(r)$.

Note that for data of finite q_{max}, the FT of the Heavyside step function is

$$sinc(r) = \sin(r)/r \quad \text{having} \quad \mathrm{FWHM}_r = 3.79/q_{\mathrm{max}}$$

so that the theoretical $\mathrm{PDF}(r)$ should be convolved with $sinc(r)$ before comparison to data. This is the source of the "low-r wiggles" in the FTs of diffraction data, which in fact exist around all sharp peaks in $\mathrm{PDF}(r)$.

Two problems for deconvolving diffraction data

Now take another look at the formula for convolution:

$$f(q)\otimes g(q) = (f\otimes g)(q) = \int_{-\infty}^{\infty} f(q')\, g(q-q')\, dq'$$

$\Rightarrow$ there are two problems in applying the convolution theorem

$$g(q) = \mathrm{FT}[\,\mathrm{FT}(I(q))\ /\ \mathrm{FT}(f(q))\,]$$

to real diffraction data:

First problem: We need data of infinite q-range for $g(q)$ and hence for the measured $I(q)$, as well as an infinite q-range for perfect knowledge of the resolution function $f(q)$. None of this is possible in practice.

Second problem: The resolution function shape or profile $f(q')$ must be independent of the argument q of $g(q-q')$. In other words, the resolution function should have the same shape at all $q = 4\pi/\lambda\ \sin(\theta)$, where 2θ is the diffraction angle. We will see from Caglioti that the resolution function FWHM depends strongly on 2θ.

The Debye-Waller factor revisited in *q*-space

The D-W factor is a (Gaussian-like) modulation of intensity in *q*-space, whose reduction of Bragg peak intensity at higher temperature is particularly noticeable when diffraction data are taken up to high-*q*:

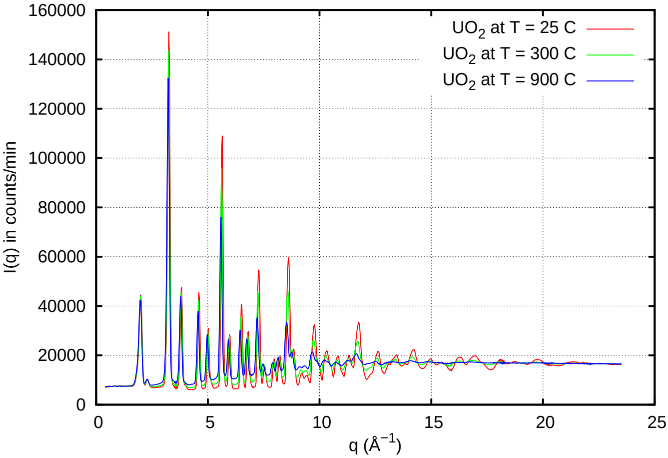

Such reduction in signal at "high harmonics" in *q* should, after Fourier transform, lead to broader features in *r*-space.

The Debye-Waller factor in *r*-space

The convolution theorem states that a modulation in *q*-space leads to a convolution in *r*-space (and vice-versa), such that the the D-W factor broadens the peaks in $\mathrm{PDF}(r)$ according to the vibration amplitudes of the corresponding atomic pairs, while preserving the peak areas which are proportional to (generally constant) coordination number:

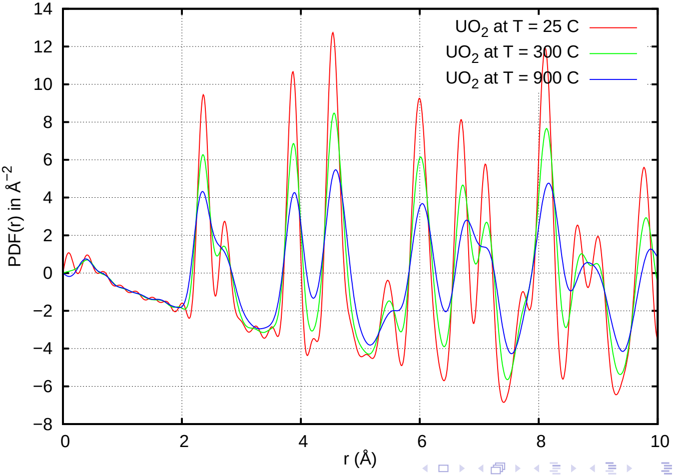

q-space versus *r*-space representations of data

Diffraction data at high $q_{\max}$ show decreasing Bragg-peak intensities due to the Debye-Waller effect (thermal averaging of atomic positions), from static disorder, and also because of limited *q*-space resolution:

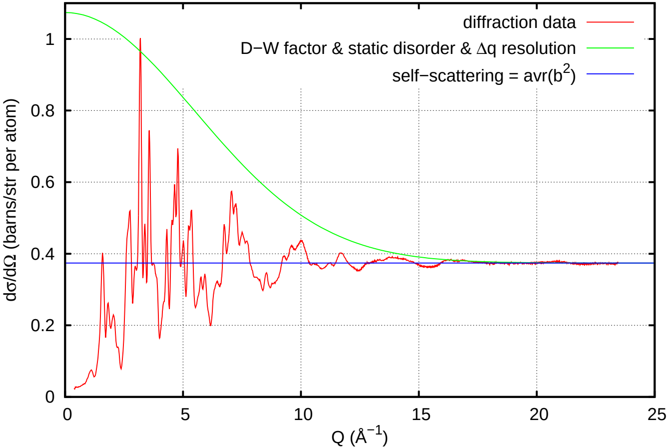

The diffraction intensity ultimately converges to the self-scattering limit $I_{\mathrm{self}} = \overline{b^2}$ when $q_{\max}$ is high enough.

q-space versus *r*-space representations of data

The diffuse scattering “underneath” the Bragg peaks, subtracted away as “background” by Rietveld refinement, contains information about dynamic disorder (*e.g.* Thermal Diffuse Scattering = TDS) and static disorder (*e.g.* lattice-constant fluctuations $\Delta a/a$). The Bragg peak widths are generally limited by the instrumental resolution Δq:

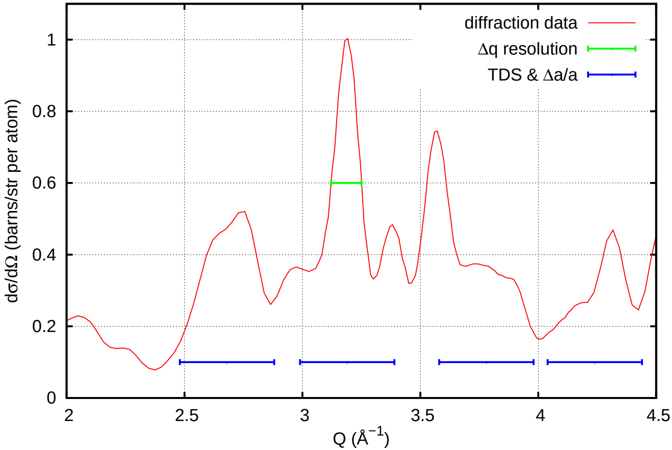

q-space versus *r*-space representations of data

Fourier transform gives the total Pair-Distribution Function $\mathrm{PDF}(r)$ for an average atom at the origin ⇒ peaks at all interatomic distances:

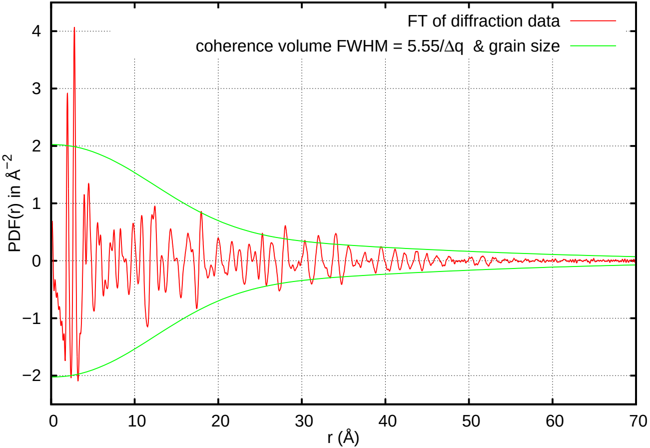

The *r*-range is limited by the grain size (*i.e.* the range of structural correlation) and by the coherence volume of the neutron that depends on the *q*-space resolution Δq.

q-space versus *r*-space representations of data

The low-r slope of a properly normalized $\mathrm{PDF}(r)$ gives ρ_0, the peak areas are proportional to coordination number for atomic pairs, whose peak widths scale with their dynamic+static disorder plus the r-space resolution function $\Delta r(r) = \mathrm{sinc}(q_{\max} r) = \sin(q_{\max} r)/(q_{\max} r)$ that also leads to non-physical FT ripples or "wiggles" at low-r:

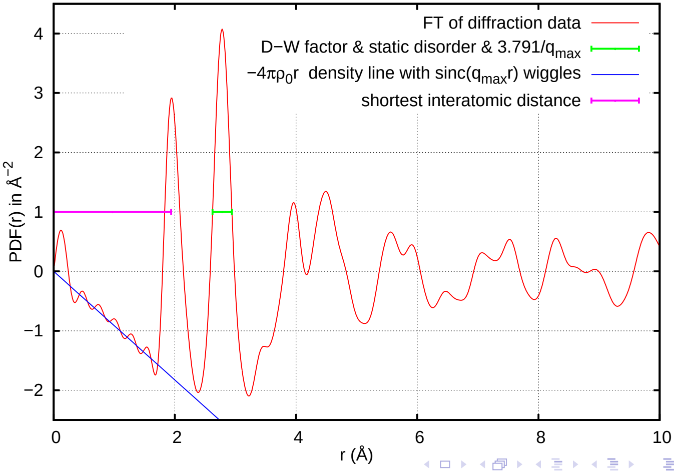

Total scattering versus Bragg peak refinement

Refinement (*e.g.* Rietveld) of Bragg peak intensities ignores both the elastic ($\omega = 0$) diffuse scattering between peaks due to static disorder as well as the inelastic scattering due to dynamic disorder, and therefore provides only a space+time averaged picture of the sample's structure.

By comparison, making use of all the measured intensity $d\sigma/d\Omega$ in a "total scattering" data analysis provides (ensemble-averaged) information on the local quasi-instantaneous structure in the sample. *Recall that a liquid has no perfectly elastic scattering intensity.*

Neither can however distinguish between static and dynamic disorder, other than by looking at the temperature dependence. For example, the D-W factor amplitude extracted from fits to either Bragg peaks or $\mathrm{PDF}(r)$ should, when extrapolated to $T = 0$ K, be very small and correspond to zero-point motion when there is no static disorder.

One can also measure the elastic scattering intensity $S(q, \omega \sim 0)$ as a function of T to see the onset of atomic motion at the time-scale of the scattered neutron's coherence time $\tau_{\mathrm{coh}} = \hbar/\delta E$, where δE is the instrumental energy resolution. The FT of $S(q, \omega \sim 0)$ (*e.g.* measured at IN1-TAS) then produces a pair-distribution function $\mathrm{PDF}(r, t \to \infty)$ of time-averaged local structures, *i.e.* showing only static correlations.

Combining Rietveld refinement and PDF-analysis

The space+time averaged picture obtained via Rietveld analysis of powder diffraction data is generally the most useful for determining the crystal structure of the sample, when this is not already known.

If the diffractometer has a high enough $q_{\max}$ (say 20 Å^{-1}), and all data corrections can be made for instrument background, sample attenuation, multiple scattering and inelasticity effects, then the same data can be used for PDF-analysis in order to probe local deviations (static or dynamic) away from the space+time averaged structure.

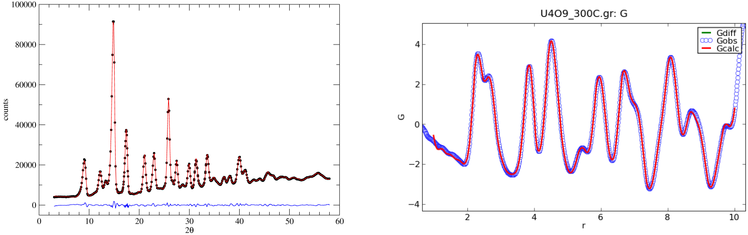

Above are $S(\mathbf{q})$ data acquired on the D4c diffractometer for disordered materials (ILL) using $\lambda = 0.5$ Å $\Rightarrow q_{\max} = 24$ Å^{-1} that have been Rietveld refined in *q*-space (left) and whose $\mathrm{PDF}(r)$ after Fourier transform has been modelled with *PDFgui* software in *r*-space (right).

Vibration modes seen by Rietveld vs PDF-analysis

Whereas Rietveld refinement gives time-averaged distances between atomic pairs, PDF-analysis sees an ensemble-average of quasi-instantaneous atomic positions and relative distances:

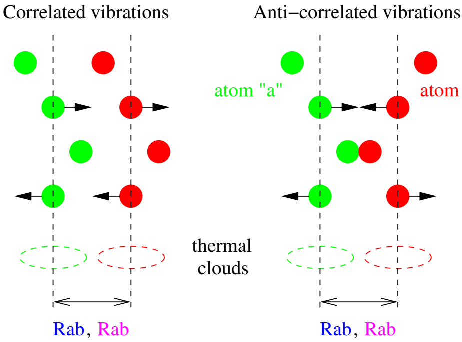

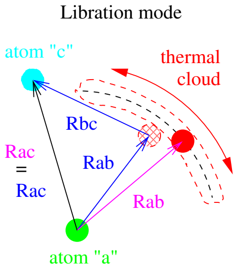

Rietveld–refined Rab = PDF–analysed Rab for both correlated and anti–correlated vibrations, but Rietveld's time–averaged thermal clouds cannot distinguish between the two cases. PDF(r) will however show a broader peak for the a–b atomic pair in the anti–correlated case.

The time–averaged position of atom b is the barycenter of its banana–shaped thermal cloud, which is closer to atom a than any instantaneous position:

Rab (too short) < Rab (correct)

PDF(r) will show a sharp peak for the a–b and a–c atomic pairs but a very broad peak for b–c.

Effect of correlated atomic vibrations at low-*r*

At short interatomic distances the peaks in $\mathrm{PDF}(r)$ are sharper and taller (conserving area ∝ coordination number) as compared to the neutron coherence volume's $\mathrm{FWHM} \sim$ 60 Å for the D4c diffractometer:

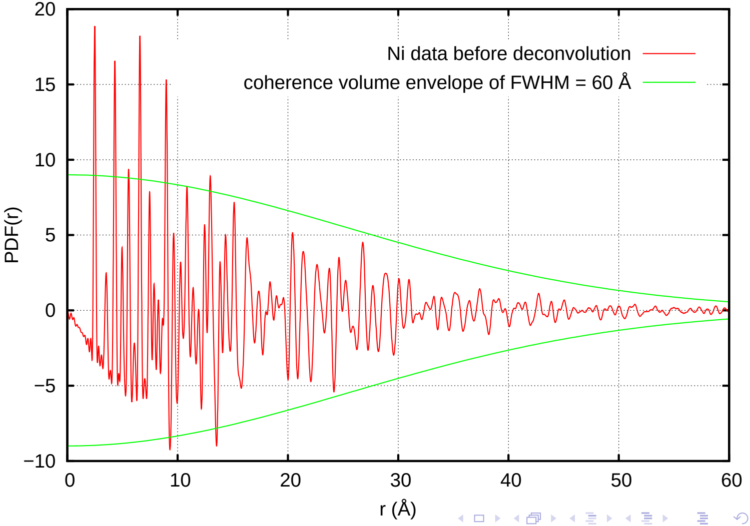

The myth of "scattering power"

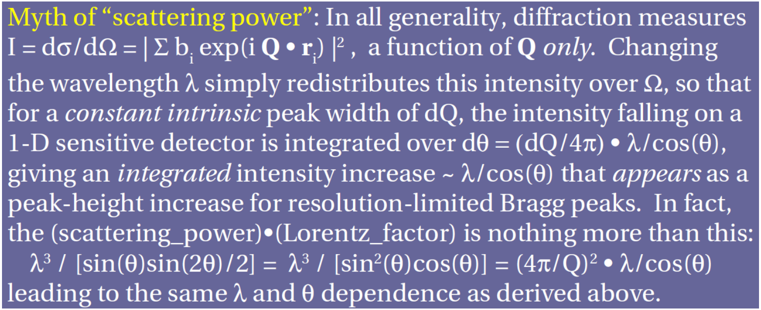

Myth of "scattering power": In all generality, diffraction measures $I = d\sigma/d\Omega = |\,\Sigma\, b_i \exp(i\,\mathbf{Q} \bullet \mathbf{r}_i)\,|^2$, a function of **Q** *only*. Changing the wavelength λ simply redistributes this intensity over Ω, so that for a *constant intrinsic* peak width of dQ, the intensity falling on a 1-D sensitive detector is integrated over $d\theta = (dQ/4\pi) \bullet \lambda/\cos(\theta)$, giving an *integrated* intensity increase ~ $\lambda/\cos(\theta)$ that *appears* as a peak-height increase for resolution-limited Bragg peaks. In fact, the (scattering_power)•(Lorentz_factor) is nothing more than this:

$$\lambda^3 / [\sin(\theta)\sin(2\theta)/2] = \lambda^3 / [\sin^2(\theta)\cos(\theta)] = (4\pi/Q)^2 \bullet \lambda/\cos(\theta)$$

leading to the same λ and θ dependence as derived above.

How many powder diffractionists understand this?

Disorder can mean more information, not less

For an ergodic system like a monoatomic fluid at temperature T, and in the low-density limit, a *classical* mean-field theory relates $g(r)$, obtainable from diffraction, to the interatomic pair potential:

$$u(r) = -k_B T \ln[g(r)],$$

from which follows the interatomic force $\mathbf{F}(r) = -\vec{\mathrm{grad}}[u(r)]$, and thereby v_{sound}, etc. For realistic densities, an iterative procedure leads to an effective pair potential $u_{\mathrm{eff}}(r)$ (*e.g.* EPSR analysis).

In effect, the distribution of interatomic distances given by $g(r)$ in a liquid or glass "probes" the shape of $u(r)$, since energetically unfavorable distances will be more rare than favorable ones. By contrast, diffraction measurements on a crystalline sample cannot give information about $u(r)$ without recourse to modelling.

Note that the above expression also implies that $g(r)$, the structure measured via diffraction, is *independent of atomic mass* in a classical picture. Any observed differences in structure, *e.g.* between the $(d\sigma/d\Omega)(\mathbf{q})$ of H_2O vs D_2O as measured by x-ray diffraction, are necessarily due to QM effects.

Q→R-space:
PDF-analysis

Henry E. Fischer

Diffraction basics
fundamental concepts
crystal diffraction
D-W and TDS
Patterson function

aPDF-analysis
total scattering
S(q) and g(r)
convolution/resolution
q-space vs *r*-space
PDF vs Rietveld
aPDF review

aPDF examples
carbon
$\mathrm{ZnSe}_{1-x}\mathrm{Te}_x$
$\mathrm{BaTi}_{1-x}\mathrm{Zr}_x\mathrm{O}_3$
UO_2

mPDF-analysis
formalism
generaliities
modeling/simulation

mPDF examples
$\mathrm{SrGd}_2\mathrm{O}_4$
$\mathrm{Gd}_2\mathrm{O}_3$
$\mathrm{Gd}_2\mathrm{Ir}_2\mathrm{O}_7$
EuPtGe
mPDF conclusions

Table of Contents

Atomic PDF-analysis: FT of a powder diffractogram

Disordered, nano-structured or reduced-dimensional crystals often lack sufficient long-range order to produce sharp diffraction peaks. It is then advantageous to sacrifice *q*-space resolution by using short wavelengths to provide a high $q_{\max}$ and thus better *r*-space resolution $\Delta r = 3.79/q_{\max}$ after Fourier Transform (FT) of the diffraction pattern taken as $d\sigma/d\Omega - \mathrm{self\_scattering}$.

The resulting Pair-Distribution Function $\mathrm{PDF}(r)$ is the distribution of relative interatomic distances with respect to an average atom at the origin (*i.e.* an ensemble of quasi-instantaneous local structures $\neq$ the time+space averaged structure from Rietveld).

Instrumental *q*-space resolution Δq determines the quantum's coherence volume seen as an envelope that modulates and limits the spatial extent of the $\mathrm{PDF}(r)$ via $r_{\max} = (5.55/2)/\Delta q$.

NB: The $\mathrm{PDF}(r)$ is not the output of structural refinement, and is therefore a *model-independent* result that can of course then be used as input for structural modelling/simulation in *r*-space, thus concluding the technique of (atomic) "**PDF-analysis**".

Atomic PDF(r) examples

PDF analysis at D4@ILL: different forms of carbon

Q-space: **R-space:**

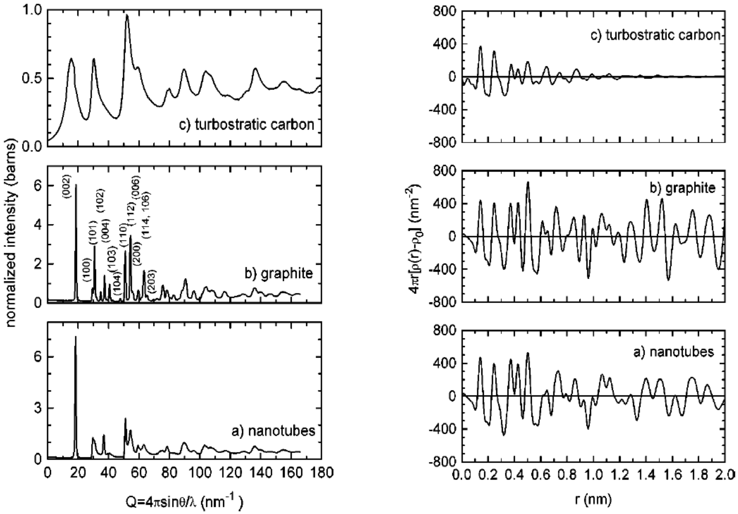

A. Burian, J.C. Dore, H.E. Fischer and J. Sloan, Phys. Rev. B **59** *(1999) 1665–8 (***60** *citations).*

Local atomic strain in $ZnSe_{1-x}Te_x$

The **q**-space Bragg peak data (left) show no sign of local strain or static interatomic distance fluctuations, but only the expected shift (from top to bottom) in average lattice constant as the smaller Se atom replaces the larger Te. The $\mathrm{PDF}(r)$ data (right) show however that the intermediate stoichiometries have significant local disorder, and that there are two distinct distances for Se-Zn ($\sim$ 2.45 Å) and Te-Zn ($\sim$ 2.63 Å).

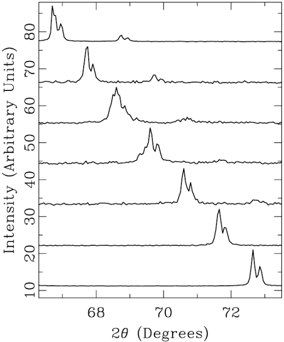

FIG. 1. ⟨331⟩ and weak ⟨420⟩ peaks of $ZnSe_{1-x}Te_x$ at (from top to bottom) $x=1, \frac{5}{6}, \frac{4}{6}, \frac{3}{6}, \frac{2}{6}, \frac{1}{6}, 0$ measured at 300K using Cu rotating anode.

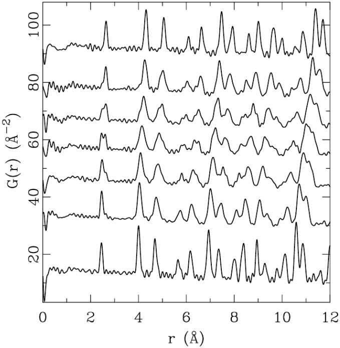

FIG. 3. $G(r)=4\pi r(\rho(r)-\rho_0)$ for $ZnSe_{1-x}Te_x$ at (from top to bottom) $x=1, \frac{5}{6}, \frac{4}{6}, \frac{3}{6}, \frac{2}{6}, \frac{1}{6}, 0$ measured at 10K.

P.F. Peterson, et al, *Phys. Rev. B* **63** *(2001) 165211.*

Local structure in $BaTi_{1-x}Zr_xO_3$ relaxors

Bragg peak refinement shows that $BaTi_{1-x}Zr_xO_3$'s crystallographic structure is ABO_3 cubic perovskite for $x = 0$ and over the relaxor ferroelectric range $(0.25 \leq x \leq 0.5)$ which includes the null-alloy composition $x = 0.32$. As charge disorder is minimized by the isovalent substitution Ti^{4+}/Zr^{4+}, it can be hypothesized that the long-range ferroelectric order is impeded by local structural distortions resulting from the large difference in the two cationic radii.

$\Rightarrow$ PDF-analysis using $\lambda = 0.5$ Å gave unambiguous evidence that the Ti and Zr atoms do not occupy equivalent octahedral sites as expected from the crystallographic structure, but rather the Ti atoms are displaced along [111].

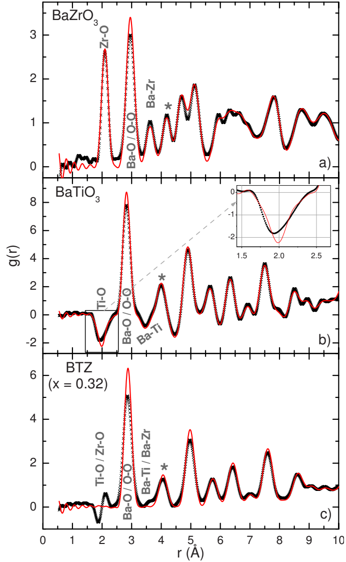

C. Laulhé, et al, *Phys. Rev. B* **79** *(2009) 064104.*

Dynamic local Pa-3 symmetry in UO_2? (D4@ILL)

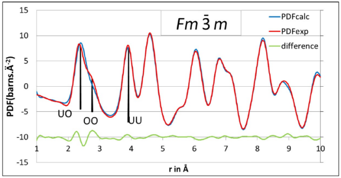

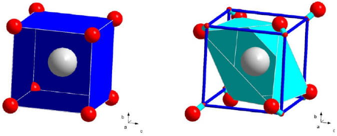

Figure 1. Uranium polyhedron coordination in *Fm*3̄*m* (left) and *Pa*3̄ (right). Uranium and oxygen atoms are colored gray and red, respectively.

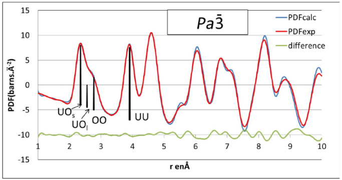

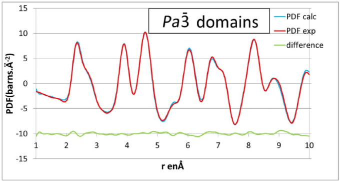

PDF-analysis of UO_2 at 1273 K reveals an asymmetric first-neighbor U-O peak, expected from anharmonic atomic vibrations, that could be explained by *dynamically* correlated O-atom displacements with local Pa-3 symmetry, *i.e.* lower than the space+time averaged Fm-3m symmetry. In any case, the O vibration amplitudes are quite large.

L. Desgranges, et al, *Inorg. Chem.* **56** *(2017) 321.*

R.I. Palomares, et al, *Phys. Rev. Mat.* **3** *(2019) 053611.*

Magnetic PDF-analysis

Generalizing to magnetic total scattering

Recall the total (nuclear) differential scattering cross-section per atom:

$$\frac{1}{N}\frac{d\sigma}{d\Omega} = \bar{b}^2\,[S(Q)-1] + \overline{b^2}$$

which comprises a “distinct” term (interference between different atoms) and a “self” term $\overline{b^2}$ (self-interference from individual atoms). As first derived by Blech and Averbach (1964), the total *magnetic* differential scattering cross-section per atom for a system of *N* identical spins is:

$$\left.\frac{1}{N}\frac{d\sigma}{d\Omega}\right|_{\mathrm{m}} = p^2\mu^2 f^2(Q)$$

$$\cdot\left\{\frac{2}{3} + \frac{1}{N}\sum_{i\neq j}\left[A_{ij}\frac{\sin(Qr_{ij})}{Qr_{ij}} + B_{ij}\left(\frac{\sin(Qr_{ij})}{(Qr_{ij})^3} - \frac{\cos(Qr_{ij})}{(Qr_{ij})^2}\right)\right]\right\},$$

where μ is the atomic magnetic moment in units of Bohr magnetons μ_{B}, $p = \gamma_n r_e/2 = 2.696$ fm, $f(Q)$ is the magnetic form factor with $f(0) = 1$, and A_{ij} and B_{ij} are spin-spin orientational correlation functions for spin components respectively perpendicular (*i.e.* transverse) or parallel (*i.e.* longitudinal/collinear) to the interspin vector $\mathbf{r}_{ij} = \mathbf{r}_j - \mathbf{r}_i$.

Generalizing to magnetic total scattering

Now define the neutron magnetic scattering length (unpolarized case):

$$b_{\mathrm{m}}(Q) \overset{\mathrm{def}}{=} \sqrt{\frac{2}{3}}\, p\, \mu\, f(Q)$$

The magnetic self-scattering per atom of the magnetic species is then:

$$\left.\frac{d\sigma}{d\Omega}\right|_{\mathrm{m,self}} = b_{\mathrm{m}}^2(Q) = \frac{2}{3} p^2 \mu^2 f^2(Q)$$

and corresponds to the magnetic diffraction intensity per spin in the absence of orientational correlations between neighboring spins. Such a sample with zero spin-spin correlations is simply in the paramagnetic state. Since we are interested precisely in the correlations between magnetic spins, we subtract the magnetic self-scattering from the total magnetic differential scattering cross-section to obtain:

$$I_{\mathrm{m}}(Q) \overset{\mathrm{def}}{=} \frac{1}{N} \left.\frac{d\sigma}{d\Omega}\right|_{\mathrm{m}} - b_{\mathrm{m}}^2(Q)$$

$$= p^2 \mu^2 f^2(Q) \cdot \frac{1}{N} \sum_{i \neq j} \left[A_{ij} \frac{\sin(Qr_{ij})}{Qr_{ij}} + B_{ij} \left(\frac{\sin(Qr_{ij})}{(Qr_{ij})^3} - \frac{\cos(Qr_{ij})}{(Qr_{ij})^2} \right) \right].$$

The magnetic Pair-Distribution Function mPDF(r)

Recall that the atomic PDF(r) is obtained by Fourier transform of $S(Q)-1$, namely the diffraction intensity $d\sigma/d\Omega$ per atom after subtraction of the self-scattering $\overline{b^2}$ and division by $\overline{b}^2$:

$$\mathrm{PDF}(r) \;=\; \frac{2}{\pi}\int_0^\infty Q\,[S(Q)-1]\,\sin(Qr)\,dQ \;=\; \frac{1}{N}\sum_{i\neq j}^{N}\frac{1}{r}\delta(r-r_{ij})\;.$$

Likewise the normalized self-scattering-subtracted magnetic diffraction intensity $I_{\mathrm{m}}(Q)$ can also be analytically Fourier transformed (first done by B.A. Frandsen, *et al* in 2014) to produce the *model-independent* magnetic Pair-Distribution Function or mPDF(r):

$$\mathrm{mPDF}(r) \overset{\mathrm{def}}{=} \frac{2}{\pi}\int_0^\infty Q\,\frac{I_{\mathrm{m}}(Q)}{\frac{2}{3}p^2\mu^2}\,\sin(Qr)\,dQ$$

$$\approx \frac{3}{2}\cdot\frac{1}{N}\sum_{i\neq j}\left[\frac{A_{ij}}{r}\tilde{\delta}(r-r_{ij})+B_{ij}\frac{r}{r_{ij}^3}\left[1-\tilde{\Theta}(r-r_{ij})\right]\right],$$

that represents both static and dynamic local spin-spin correlations, where the delta-function $\tilde{\delta}(r-r_{ij})$ and the Heaviside step function $\tilde{\Theta}(r-r_{ij})$ have been broadened by $\mathrm{FWHM}_{\mathrm{R}} \approx 4\ln(4)/\mathrm{FWHM}_{f^2(Q)}$ since we chose for experimental reasons not to divide $I_{\mathrm{m}}(Q)$ by $f^2(Q)$.

Generalities about magnetic PDF-analysis

For non-polarized neutron diffraction from 1 pair of F or AF magnetic spins, $f(r) = \mathrm{mPDF}(r)$ clearly indicates whether the spins' orientation is transverse (showing a strong peak) or longitudinal/collinear (showing a strong slope at low-r) with respect to the interspin vector $\mathbf{r}_{ij} = \mathbf{r}_j - \mathbf{r}_i$.

ferromagnetic:

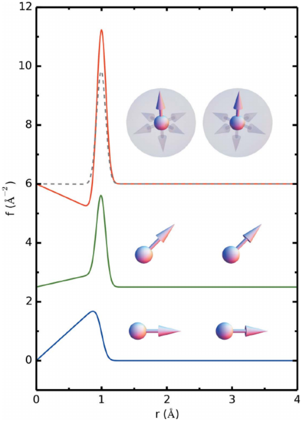

anti-ferromagnetic:

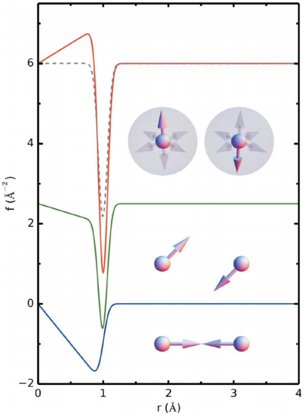

B.A. Frandsen, et al, *Acta. Cryst. A* **70** *(2014) 3–12.*

Generalities about magnetic PDF-analysis (cont'd)

In 1D and 3D systems, transverse versus collinear magnetic structures for F/AF can generally be distinguished respectively by positive/negative peaks versus positive/negative low-*r* slopes in the mPDF(*r*), except in the case of rotational invariance imposed by cubic lattice symmetry.

AF 1-D chain of spins:

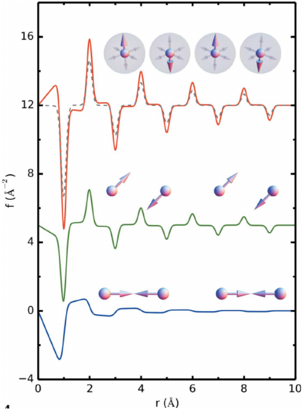

AF 3-D cubic structure:

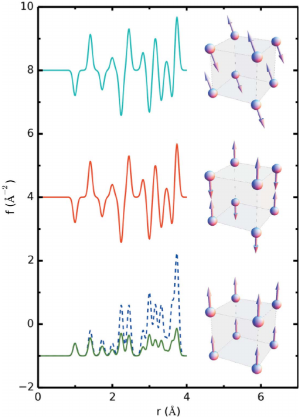

B.A. Frandsen, et al, *Acta. Cryst. A* **70** *(2014) 3–12.*

Modeling techniques for Magnetic PDF-analysis:

Small box modeling (*e.g.* the diffpy.mpdf module for DiffPy-CMI) :

- R-space based *refinement* of spin orientations and perhaps other parameters to fit the measured mPDF(r) – similar to PDFgui, MolPDF.
- Small number of spins, perhaps only one magnetic unit cell.
- Qmax and Qmin are inputed to simulate experimental conditions.
- Additional parameters to dampen and/or broaden the mPDF, simulating the effects of thermal motion and instrumental resolution.

⇒ Runs fast, fits directly the mPDF(r), but susceptible to mixing instrumention effects with structural features.

Large box modeling (*e.g.* Spinvert, RMCprofile) :

- Q-space based *Reverse Monte Carlo* simulation of spin orientations to fit the measured magnetic diffuse scattering $I_{\rm m}(Q)$.
- Large number (thousands) of spins, corresponding to the dimensions of the neutron coherence volume.
- The fit to $I_{\rm m}(Q)$ is FT-ed to produce the simulated mPDF(r).

⇒ Accurately treats instrumention effects, can smooth out noisy data, permits sampling of spin-spin correlation functions, but runs more slowly and can be susceptible to maximum-entropy effects and local minima.

Magnetic PDF(r) examples

Nuclear structure of $SrRE_2O_4$ (*Pnma*, No. 62)

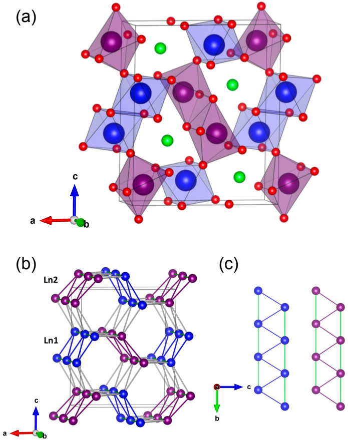

(a) The orthorhombic unit cell of the $SrRE_2O_4$ structure. The magnetic RE ions occupy two distinct 4*c* Wyckoff sites having octahedral O-coordination and forming around Sr atoms distorted hexagons. (b) The *distorted honeycomb structure* of the magnetic ions manifests along the *b*-axis two types of *zig-zag ladders* (shown in (c)) containing triangles that induce a large degree of *geometrical frustration* due to the NN anti-ferromagnetic exchange.

The two slightly different crystallographic environments of the RE ions at two distinct 4*c* Wyckoff sites $(x, \frac{1}{4}, z)$ leads to different magnetic ordering in the case of strong CEF effects. Rietveld results (D20@ILL) show that $SrGd_2O_4$ exhibits *longitudinal F* order along each 1D chain but AF correlations between the two chains of a given zig-zag ladder.

Diffraction data for $SrGd_2O_4$ (D4c@ILL, $\lambda = 0.5$ Å)

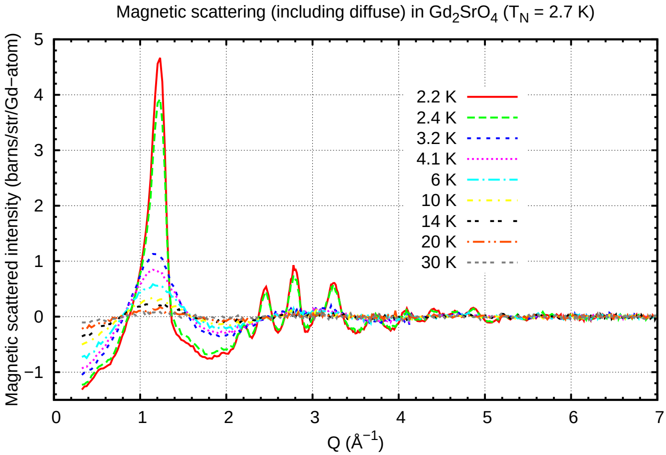

After subtraction of a 50 K “paramagnetic baseline”, representing the *Q*-dependent magnetic self-scattering, and normalization via vanadium to an absolute diffraction intensity scale as $d\sigma/d\Omega$.

mPDF(r) data for $SrGd_2O_4$ (D4c@ILL $\lambda = 0.5$ Å)

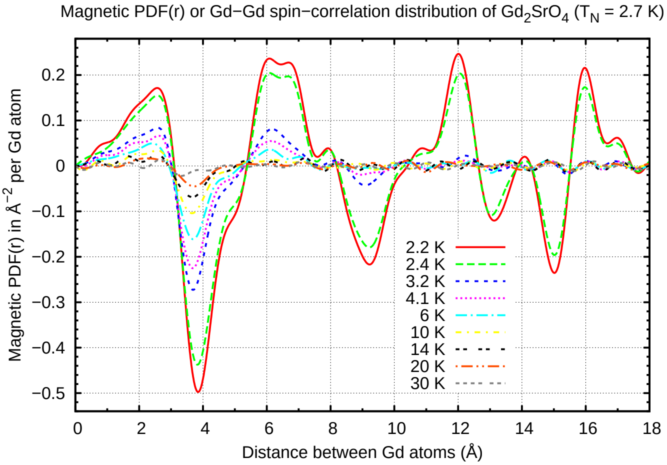

Fourier transform for $Q_{\text{max}} = 7$ $Å^{-1}$ after dividing by the magnetic self-scattering $\frac{2}{3}p^2\mu^2$ (*i.e.* sans form factor squared $f^2(Q)$).

Reverse Monte Carlo simulations using SPINVERT

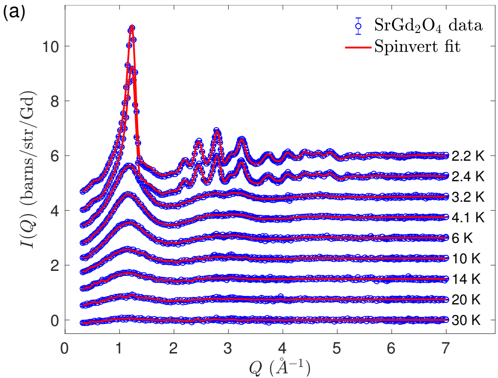

RMC simulations using SPINVERT* fit well the intensity-normalized, 50K-subtracted magnetic diffraction data in *Q*-space ($T_N = 2.7$ K). Ising spins $\|$ *b* are used in a simulation box of 9 x 27 x 9 unit cells that corresponds to the $\sim$ 60 Å spherical neutron coherence volume, and thus to the *Q*-space resolution, of the D4c neutron diffractometer.

J.A.M. Paddison,* et al, *J. Phys.: Condens. Matter* **25 *(2013) 454220.*

r-dependence of the spin-spin correlations

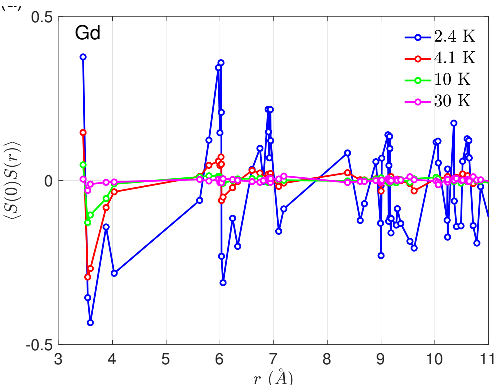

The simple dot-product spin-spin correlation function $\langle \mathbf{S}(0) \cdot \mathbf{S}(r) \rangle$, obtained from the RMC fits, gives the ensemble-averaged alignment between two identifiable spins at a given instant, as separated by the interspin distance r, independent of the direction of the interspin vector $\mathbf{r}_{ij} = \mathbf{r}_j - \mathbf{r}_i$. Clearly observable well above T_N are some short-range *dynamic* spin-spin correlations. Strong correlations at large r indicate long-range *static* correlations (*i.e.* magnetic order) that set in below T_N.

T-dependence of the spin-spin correlations

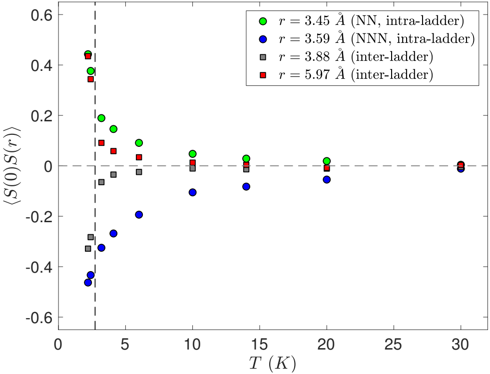

$\langle \mathbf{S}(0)\cdot\mathbf{S}(r)\rangle$ can be obtained from the RMC fits for selected intra-chain, inter-chain (*i.e.* intra-ladder) & inter-ladder distances as a function of T. Strong *intra*-ladder correlations (circles) are observed far above T_N (vertical dashed line). *Inter*-ladder correlations (squares) become important only a few K above T_N. All spin-spin correlations are increasingly dynamic as $T > T_N$, and static as $T < T_N$ (dashed line).

mPDF(*r*) derived analytically and from RMC fits

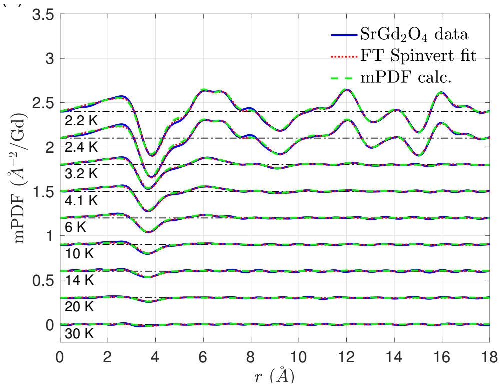

The analytical calculations of the mPDF(*r*) make use of the spin configurations generated by Spinvert, from which are calculated the A_{ij} and B_{ij} spin-spin orientational correlation functions. The strong positive low-*r* slope confirms the longitudinal F-correlations along 1D chains. The broad negative peak shows the AF correlations between both inter-chain ($r \sim 3.6$ Å) and inter-ladder ($r \sim 3.9$ Å) spins. The positive ~ 6 Å peak indicates ferro NNN-correlations within a hexagon.

D4c and Spinvert results for Gd_2O_3 (monoclinic)

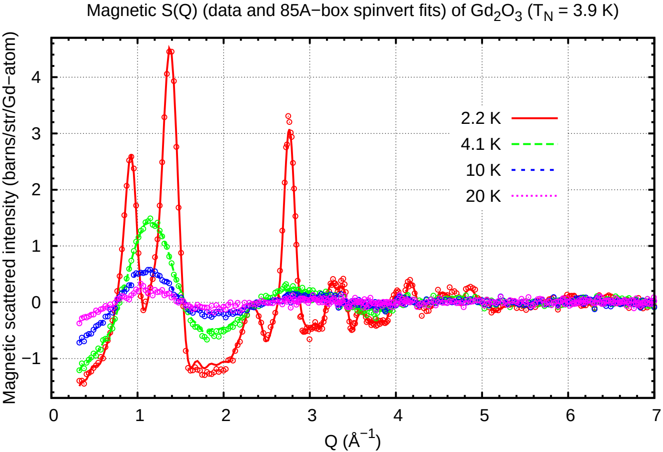

Some quick measurements of magnetic diffraction intensity for the "impurity phase" Gd_2O_3 produced some intriguing results. (Here shown after subtraction of a 50 K "paramagnetic baseline").

Possible metastable spin configurations above T_N?

Magnetic PDF(r) (data and 85A−box spinvert fits) of Gd_2O_3 (T_N = 3.9 K)

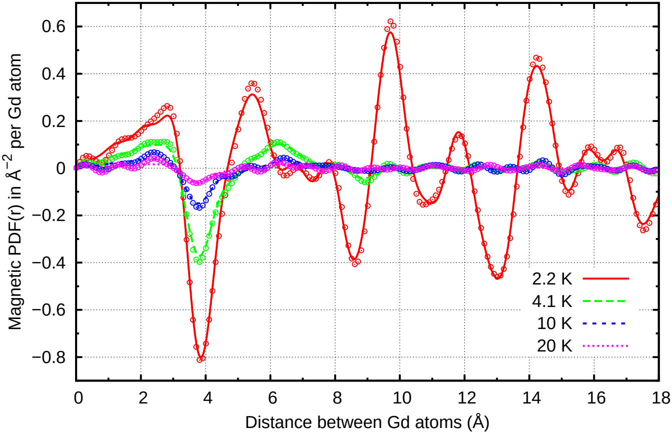

The PDF(r) from the 3D-constrained Spinvert RMC fits in Q-space reproduce the anomalous features at $r = 6$ Å and $r = 9$ Å for $T = 4.1$ K (green curve), corresponding to inter-spin distances that do not show significant correlations in the ordered magnetic structure below T_N.

Magnetic PDF-analysis of the pyrochlore $Gd_2Ir_2O_7$

Total magnetic scattering in *q*-space (c) and *r*-space (d, 3K-50K):

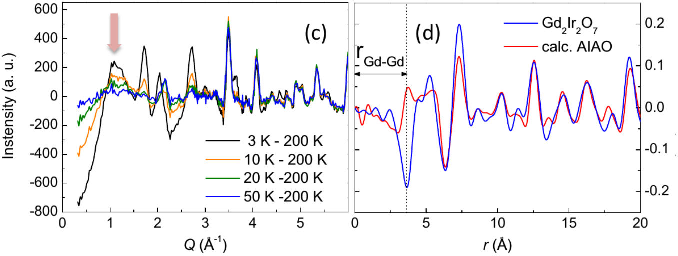

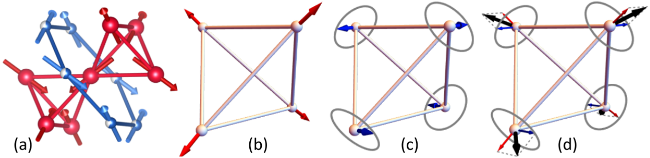

The mPDF(r) results from D4 allowed to conclude that the Gd magnetic structure at low-T in this geometrically frustrated material (d) manifests a coexistence of AIAO (a,b) and Palmer-Chalker (c) configurations.
E. Lefrançois, et al, *Phys. Rev. B* **99** *(2019) 060401(R).*

F vs AF correlations in EuPtGe (cubic $P2_13$, # 198)

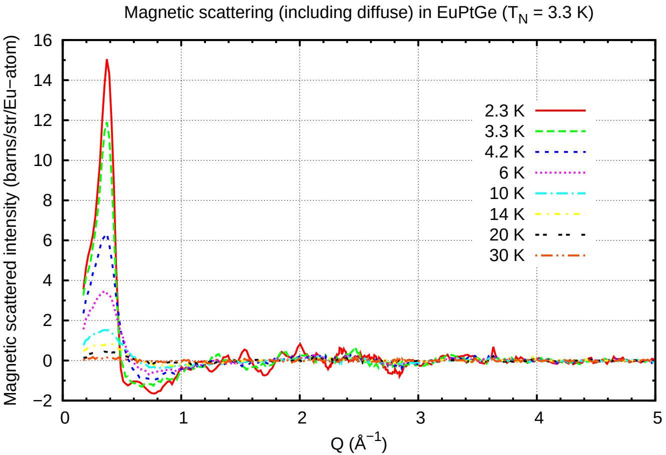

Puzzle : First-order magnetic transition to AF at $T_{\mathrm{N}} = 3.3$ K but $\Theta_{\mathrm{CW}} > 0$ from high-T susceptibility, hence predominantly F interactions. Specific heat shows spin entropy is recovered only at several times T_{N}, implying strongly correlated spin fluctuations.

mPDF(r) data for EuPtGe (D4c@ILL, $\lambda = 0.7$ Å)

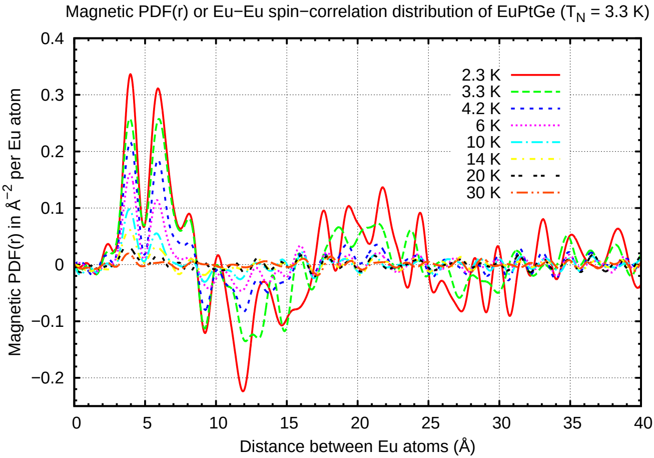

Quick semi-quantitative analysis of the mPDF(r) suggests a helical structure ($\sim$ 17 Å period) of Eu^{2+} spins correlated F within a given plane $\perp$ **k**, producing zero net F-ordered moment after *n* planes.

NB: Low-*T* helical phase found in EuPt**Si** from ND/single-crystal: *K. Kaneko*, et al, *J. Phys. Soc. Jpn.* **88** *(2019) 013702.*

Conclusions for magnetic PDF-analysis

Magnetic diffuse total-scattering as measured by neutron diffraction provides quantitative information on short-ranged spin-spin correlations that can be either static (below T_N) or dynamic (above T_N). In contrast, Rietveld refinement provides structural information only as averaged over time and space, very useful for crystallography.

By imposing a physical 3D model of the magnetic system, RMC simulations of magnetic diffuse scattering data allow to derive in a robust way the real-space spin-spin correlation function $\langle \mathbf{S}(0) \cdot \mathbf{S}(r) \rangle$ as a function of interspin distance and temperature, even when the diffraction data are beset by significant statistical noise.

Magnetic PDF-analysis provides a *model-independent* real-space function mPDF(r), obtained directly from the diffraction data, that permits to distinguish longitudinal vs transverse spin-spin correlations, albeit with limited R-space resolution due to the magnetic form factor.

The complementary use of RMC simulations with mPDF-analysis of magnetic diffuse scattering data offers a powerful tool for investigating both static and dynamic spin-spin correlations in disordered magnetic systems, such as those subject to geometrical frustration.

Table of Contents